# Uptake of Gas-Phase Ammonia. 1. Uptake by Aqueous Surfaces as a Function of pH

**Q. Shi and P. Davidovits***

*Department of Chemistry, Merkert Chemistry Center, Boston College, Chestnut Hill, Massachusetts 02167-3809*

**J. T. Jayne, D. R. Worsnop, and C. E. Kolb**

*Center for Aerosol and Cloud Chemistry, Aerodyne Research, Inc., Billerica, Massachusetts 01821-3976*

*Received: May 24, 1999; In Final Form: August 16, 1999*

The uptake of gas-phase ammonia by aqueous surfaces was measured as a function of temperature, gas liquid interaction time, and pH in the range 0−13. Uptake measurements at low pH yielded values of the mass accommodation coefficient ($\alpha$) as a function of temperature. The mass accommodation coefficient increases as the temperature decreases, from 0.08 at 290 K to 0.35 at 260 K. Time dependence of the uptake yielded values for the Henry's law constant. Uptake measurements at high pH indicate that an ammonia surface complex is formed at the interface. Codeposition studies in which an aqueous surface, initially at pH = 4, was simultaneously exposed to both gas-phase ammonia and $SO_2$ were also performed. In such a codeposition experiment, the species entering the liquid neutralize each other and as a result the uptake of each species is enhanced. Modeling calculations indicate that the uptake of each species is in accord with bulk liquid-phase kinetics.

## Introduction

Ammonia in the atmosphere originates primarily from ground sources including decaying organic matter and chemical fertilizers. Significant amounts of $NH_3$ (0.1−100 ppbv) are found in both clean and polluted atmospheres as well as in cloud and fog droplets.[1] Since ammonia is the only soluble base found in the atmosphere in significant quantities, it plays a principal role in neutralizing acidic aerosols ($H_2SO_4$, $HNO_3$, and HCl) converting them to new nonvolatile or semivolatile components; $(NH_4)_2SO_4$, $NH_4HSO_4$, $NH_4NO_3$, $NH_4Cl$.[2] The process of neutralization influences the aqueous oxidation rates of S(IV) species. A recent study by Meng et al.[3] found that atmospheric ammonia is an important precursor for aerosol formation in the Los Angeles area.

Gas-phase reactions involving $NH_3$ are slow.[4] Tropospheric lifetime for reaction with OH radical for example, is typically about 3 months, and tropospheric photolysis is negligible.[5] Therefore, uptake by aerosols and liquid droplets is the principal tropospheric sink for gaseous ammonia and heterogeneous interactions of $NH_3$ are of significant interest to atmospheric chemists.

The uptake of gas phase ammonia by water has been previously studied in a limited range of acidities by Ponche et al.[6] at 17 °C, and Bongartz et al.[7] at 25 °C. We have completed a series of $NH_3$−liquid water and the $NH_3$−sulfuric acid uptake measurements in two independent studies using separate droplet train apparatuses. The water studies were done as a function of pH (0−13) and temperature in the range 20 °C to −10 °C. The sulfuric acid studies were done in the range 10 to 70 wt % $H_2SO_4$ and as a function of temperature in the range 20 °C to −25 °C. The time dependence of the uptake was measured by varying the gas−liquid interaction time from 2 to 15 ms. Uptake measurements yielded values of the mass accommodation coefficient ($\alpha$) and provided information about interactions of ammonia molecules at the gas−liquid interface. In this article we present results of uptake studies on water, including codeposition studies with $SO_2$. The results of the $NH_3$−sulfuric acid uptake measurements are presented in the following companion article.[8]

## Modeling Gas−Liquid Interactions

In our droplet train apparatus, discussed in the following section, a gas phase species interacts with liquid droplets and the disappearance of that species from the gas phase is monitored. The disappearance of the species may be due to the entry of the molecules into the bulk liquid (and possibly subsequent reactions in the bulk liquid), or to a reaction of the species at the gas−liquid interface. A phenomenological description of the entry of gases into liquids is straightforward. First, the gas phase molecule is transported to the liquid surface, usually by gas-phase diffusion. The initial entry of the species into the liquid is governed by the mass accommodation coefficient $\alpha$ which is the probability that an atom or molecule striking a liquid surface enters into the bulk liquid phase.

$$\alpha = \frac{\text{no. of molecules entering the liquid phase}}{\text{no. of molecular collisions with the surface}} \quad (1)$$

In the absence of surface reactions, the mass accommodation coefficient determines the maximum flux $J$ of gas into a liquid, which is given by

$$J = \frac{n_g \bar{c} \alpha}{4} \quad (2)$$

If reactions occur at the gas−liquid interface, then the flux of species disappearing from the gas phase may exceed that given by eq 2.

10.1021/jp991696p CCC: $18.00 
Published on Web 10/14/1999

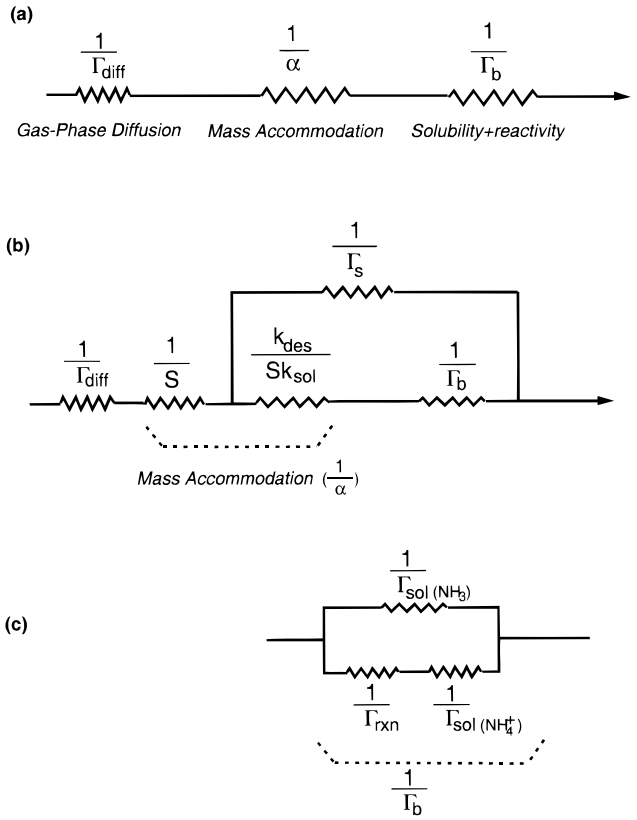


**Figure 1.** (a) Electrical circuit analogue for the gas uptake process governed by gas-phase diffusion, mass accommodation, and bulk phase solubility and reactivity. Explanation is found in the text. (b) Electrical circuit analogue for the gas uptake process including surface reactivity. (c) Expanded electrical circuit analogue for the gas uptake process in the bulk liquid phase.

In a laboratory experiment gas uptake by a liquid is usually limited by gas-phase diffusion and often by solubility constraints as the species in the liquid approaches Henry's law saturation. In the latter process, some of the molecules that enter the liquid evaporate back into gas phase due to the limited solubility of the species. At equilibrium, the liquid is saturated and the flux of molecules into the liquid is equal to the rate of desorption of these molecules out of the liquid. The net uptake is then zero. Chemical reactions of the solvated species in the bulk liquid can provide a sink for the species, reducing the effect of saturation, and this increases the species uptake from the gas phase. In experiments subject to these effects, the measured flux $J$ into a surface is expressed in terms of a measured uptake coefficient, $\gamma_{meas}$, as

$$J = \frac{n_g \bar{c} \gamma_{meas}}{4} \tag{3}$$

Since $\gamma_{meas}$ represents a convolution of the several physical and chemical processes discussed above, the experimental challenge is to separate the contributions of these processes to the overall gas uptake. The droplet train apparatus allows direct control of many of the factors affecting the rate of gas uptake and thereby enables the deconvolution of the uptake into its component processes.[9−12]

General solutions to the uptake equations, which include the effect of mass accommodation, Henry's law solubility, chemical reaction in the aqueous bulk phase and interactions at the gas−liquid interface, are not available. However, Danckwerts[13,14] and Sherwood and Pigford[15] provide solutions for three specific cases in the absence of gas-phase diffusion limitation: (1) uptake governed by mass accommodation and solubility, (2) uptake governed by mass accommodation, solubility and irreversible reaction in the bulk phase liquid, and (3) uptake governed by solubility and reversible reactions. The mass accommodation limitation on the uptake is not included in the treatment of case 3. For completeness the exact expressions for the uptake coefficient related to these three cases are presented in Appendix 1. The uptake coefficient in the absence of gas-phase diffusion limitation is designated as $\gamma_o$.

To obtain an expression for $\gamma_{meas}$ that takes into account all the factors affecting the $NH_3$ uptake, it is necessary to decouple mass accommodation from the bulk phase processes. In this vein, in the absence of surface reactions, an expression for the experimentally measured uptake coefficient $\gamma_{meas}$ is given as

$$\frac{1}{\gamma_{meas}} = \frac{1}{\Gamma_{diff}} + \frac{1}{\gamma_o} = \frac{1}{\Gamma_{diff}} + \frac{1}{\alpha} + \frac{1}{\Gamma_b} \tag{4}$$

Here $\Gamma_{diff}$ represents the effect of gas-phase diffusion and $\Gamma_b$ represents the effect of reaction and the solubility of $NH_3$ and $NH_4^+$ in the bulk liquid. Expressions for these terms will be presented in the following sections. An electrical circuit analogue for this representation is shown in Figure 1a.

Several recent gas uptake experiments,[12,16−20] including the present $NH_3$(g) uptake study, make it evident that interactions at the gas−liquid interface have a significant effect on the species uptake. The treatment of gas−liquid interactions in decoupled approximate form shown in eq 4 and Figure 1a has the important advantage of allowing convenient inclusion of surface interactions for which an adequate exact treatment is not available.

**Interfacial Processes.** Processes occurring at the gas−liquid interface can be taken into account as shown in eq 5 with surface reactions included as presented by Hanson:[21]

$$n_g \underset{k_{des}}{\overset{k_{ads}}{\rightleftarrows}} n_s \xrightarrow{k_{sol}} n_l \xrightarrow{k_{rxn}} \text{product} \qquad n_s \xrightarrow{k_{surf}} \text{product} \tag{5}$$

Here the subscripts g, s, and l represent the gas, surface, and liquid state of the species. In this representation we have omitted the reverse arrow from $n_l$ to $n_s$, because desorption out of the bulk liquid is accounted for separately by $\Gamma_b$ in eq 4. Possible surface reaction processes are included via the pseudo-first-order rate coefficient $k_{surf}$.

**Mass Accommodation.** In the absence of surface reaction (i.e., $k_{surf} = 0$), eq 5 reduces to a two step process as formulated for mass accommodation in Jayne et al. [22] and Nathanson et al.[23] First, the gas molecule strikes the surface and is thermally accommodated as the surface species $n_s$. This adsorbed surface species then either enters the liquid ($k_{sol}$) or desorbs ($k_{des}$) from the surface. The adsorption rate constant (or deposition velocity) is $k_{ads} = S\bar{c}/4$. Here $\bar{c}$ is the trace gas average thermal speed and $S$ is the adsorption coefficient, that is, the fraction of collisions that results in thermal accommodation of the trace gas onto the surface. In the absence of liquid saturation effects (desorption from the liquid), the uptake flux is expressed in terms of the incoming and outgoing fluxes as

$$\alpha n_g \bar{c}/4 = n_g S\bar{c}/4 - n_s k_{des} \tag{6}$$

and by mass conservation:

$$\alpha n_g \bar{c}/4 = n_s k_{sol} \tag{7}$$

From these relationships we obtain:

$$1/\alpha = 1/S + k_{des}/Sk_{sol} \quad (8)$$

Thus, $\alpha$ is a measure of the ratio $k_{sol}/k_{des}$ in eq 5.

**Chemical Interactions at the Interface.** Interactions specific to the gas−liquid interface open a new channel for the removal of gas-phase species distinct from the mass accommodation coefficient $\alpha$. Modifications to the circuit in Figure 1a include surface reactions which depend on the nature of the interaction at the gas−liquid interface. In one approach suggested by Hanson,[21] interactions at the gas liquid interface are taken into account by inserting the resistor $1/\Gamma_s$ between the two terms $1/S$ and $k_{des}/Sk_{sol}$ in eq 8 as shown in Figure 1b. The expression for $\gamma_{meas}$ is now

$$\frac{1}{\gamma_{meas}} = \frac{1}{\Gamma_{diff}} + \frac{1}{S} + \frac{1}{\Gamma_s + \dfrac{1}{\dfrac{S-\alpha}{S\alpha} + \dfrac{1}{\Gamma_b}}} \quad (9)$$

Here $\Gamma_s$ represents the effect on the uptake of surface processes.

At the relatively low temperature of our experiments, the adsorption coefficient $S$ is expected to be close to unity. [23,24] For simplicity, here we will assume $S = 1$. Equation 9 via eq 8 is now simplified to

$$\frac{1}{\gamma_{meas}} = \frac{1}{\Gamma_{diff}} + 1 + \frac{1}{\Gamma_s + \dfrac{1}{\dfrac{k_{des}}{k_{sol}} + \dfrac{1}{\Gamma_b}}} \quad (10)$$

We can identify two interfacial processes that are to be included in $\Gamma_s$: 1. Enhancement of uptake due to a chemical reaction of the species at the interface ($\Gamma_s^{rxn}$) and 2. enhancement of uptake due to formation of surface species or complexes ($\Gamma_s^{cx}$). The overall surface uptake coefficient $\Gamma_s$ is

$$\Gamma_s = \Gamma_s^{rxn} + \Gamma_s^{cx} \quad (11)$$

These two surface parameters are discussed below.

*Surface Chemical Reaction.* The effect on the gas uptake of surface reactions is formulated in terms of $n_s$ and $k_{surf}$ in eq 5, and the surface uptake coefficient $\Gamma_s^{rxn}$ is obtained by noting that, in the absence of bulk uptake,

$$n_g \bar{c} \Gamma_s^{rxn}/4 = n_s k_{surf} \quad (12)$$

From conditions of detailed balance at the surface we obtain

$$\frac{\bar{c}}{4} n_g = k_{des} n_s \quad (13)$$

Therefore,

$$\Gamma_s^{rxn} = k_{surf}/k_{des} \quad (14)$$

This formulation of $\Gamma_s$ is analogous to the formulation of $\alpha$ in terms of a ratio of rate constants.

*Surface Species.* Gas-phase molecules interacting with the surface form a surface specific species which, under some conditions, can lead to a measurable gas uptake. Before we examine this process, we note that in eqs 5 and 12 we identified the surface species $n_s$ with the mass accommodation process and surface reaction (if any). However, as discussed in Shi et al.,[12] the gas−liquid interface is a highly complex region within which the trace species may assume a variety of configurations, differing perhaps in the degree of hydration or orientation. Therefore, we will retain the possibility that the gas-phase molecule which strikes the liquid surface may form a complex which resides on the surface but does not participate in the mass accommodation or surface reaction processes. The total species surface density is designated as $n_s^{cx}$ ($cm^{-2}$), which includes the species $n_s$.

On the millisecond time scale of the droplet experiments, the surface species (or complex) rapidly reaches steady state or equilibrium with the gas-phase species. Therefore, the density of surface species represents a net one-time uptake of a fixed number of molecules, independent of the gas−liquid interaction time $t$. The surface uptake coefficient due to the formation of a complex at the surface is obtained from:

$$(\bar{c}/4) n_g \Gamma_s^{cx} t = n_s^{cx} \quad (15)$$

At the relatively low gas-phase densities ($10^{13}$−$10^{14}$ $cm^{-3}$) characteristic of our experiments, the liquid surface is well below saturation, and an equilibrium value for $n_s^{cx}/n_g = A^{cx}_{eq}$ (cm) can be defined.[25] Further, as in eq 13, detailed balance at the surface can be invoked to show that $n_s^{cx}/n_g = \bar{c}/4k^{cx}_{des}$. Note, since $n_s^{cx}$ may be different from $n_s$, (specifically, $n_s^{cx} \geq n_s$) $k^{cx}_{des}$ may be different from $k_{des}$ (specifically, $k_{des} \geq k^{cx}_{des}$). The uptake coefficient $\Gamma_s^{cx}$ is then given by

$$\Gamma_s^{cx} = (4/\bar{c}t)\, A^{cx}_{eq} = 1/tk^{cx}_{des} \quad (16)$$

The magnitude of $\Gamma_s^{cx}$ is relatively small, on the order $10^{-3}$, even at the shortest gas−liquid interaction times of the droplet apparatus. Its effect on the gas uptake is therefore evident only if the overall uptake coefficient $\gamma_{meas}$ is on the same order.[26] The effect of such a complex formation is in fact observed in the uptake of ammonia on high-pH (low solubility) aqueous solutions, as will be described in a following section.

**Solubility and Reactivity in the Bulk Liquid**. In this section we derive an expression for $\Gamma_b$ which takes into account the effect on gas uptake of Henry's law solubility and chemical reactions of the species in the bulk liquid. We begin with the equilibrium relationship between gas-phase $NH_3$(g) and solvated $NH_3$(aq) concentrations which is determined by the Henry's law constant $H$ ($M\ atm^{-1}$) as

$$NH_3(g) \overset{H}{\rightleftharpoons} NH_3(aq) \quad (17)$$

The Henry's law constant, H is defined as

$$[NH_3(aq)] = Hp_{NH_3} = [NH_3(g)]\, RTH \quad (18)$$

Here $R$ is the gas constant in units of atm $M^{-1}$ $K^{-1}$ and $p_{NH_3}$ is the partial pressure of ammonia (atm). In the aqueous phase, $NH_3$(aq) interacts with water and $H^+$ and in equilibrium the following relationships are in effect:

$$NH_3(aq) + H_2O \underset{k_r}{\overset{k_f}{\rightleftharpoons}} NH_4^+(aq) + OH^-(aq) \quad (K_b) \quad (19)$$

$$NH_3(aq) + H^+(aq) \underset{k_r'}{\overset{k_f'}{\rightleftharpoons}} NH_4^+(aq) \quad (K_b') \quad (20)$$

Here $K_b = k_f/k_r$ and $K_b' = k_f'/k_r'$. $K_b$ and $K_b'$ are related by $K_w$, the dissociation constant for water, as $K_b' = K_b/K_w$. The values and units for these parameters are listed in Tables 3 and 4 (Appendix 2).

The total capacity of the liquid to contain the two ammonia species can be expressed in terms of an effective Henry's law constant $H^*$ defined as

$$\{[NH_3(aq)] + [NH_4^+(aq)]\} = [NH_3(g)]RTH^* \quad (21)$$

with

$$H^* = H(1 + K_b'[H^+]) = H(1 + K_b/[OH^-]) = H + HK_b/[OH^-] \quad (22)$$

The first term in eq 22 ($H$) is the physical solubility of $NH_3$, and the second term is that of the ion $NH_4^+$. In the uptake process the effect of these two solubilities is represented by $\Gamma_{sol}(NH_3)$ and $\Gamma_{sol}(NH_4^+)$.

The extent to which the full capacity of the liquid to hold the ammonium species (designated by $\Gamma_{sol}(NH_4^+)$) is accessible to the uptake process depends on the forward reaction rates in eqs 19 and 20. The limiting effect of these reaction rates is taken into account by the term $\Gamma_{rxn}$ as shown by the expanded view of $\Gamma_b$ in Figure 1c. This conceptual formulation of $\Gamma_b$ has been verified by comparison with more exact treatments by Sherwood and Pigford (see eqs A1-5 and A1-6 in Appendix 1, and Shi[27]).

Expressions for $\Gamma_{sol}(NH_3)$, $\Gamma_{sol}(NH_4^+)$, and $\Gamma_{rxn}$ are obtained from eq A1-4 together with eq 3-12 in Danckwerts[14] by appropriate extrapolations.

$$\frac{1}{\Gamma_{sol}(NH_3)} = \frac{\bar{c}}{8RTH}\sqrt{\frac{\pi t}{D_1}} \quad (23)$$

$$\frac{1}{\Gamma_{sol}(NH_4^+)} = \frac{\bar{c}[OH^-]}{8K_bRTH}\sqrt{\frac{\pi t}{D_1}} \quad (24)$$

$$\frac{1}{\Gamma_{rxn}} = \frac{\bar{c}}{4HRT}\sqrt{\frac{1}{D_1 k_1}} \quad (25)$$

Here $D_l$ is the liquid-phase diffusion coefficient for the species. Note that eqs 23 and 24 are the integral forms of the solutions, giving the average uptake from time 0 to time $t$. In eq 25, $k_1$ is the pseudo-first-order reaction rate for the formation of $NH_4^+$ in eqs 19 and 20:

$$k_1 = k_f + k_f'[H^+] \quad (26)$$

Using circuit analysis, $\Gamma_b$ in Figure 1c can be expressed as

$$\frac{1}{\Gamma_b} = \frac{1}{\Gamma_{sol}(NH_3) + \dfrac{1}{\dfrac{1}{\Gamma_{rxn}} + \dfrac{1}{\Gamma_{sol}(NH_4^+)}}} \quad (27)$$

Under the conditions of our ammonia uptake experiments, the decoupled expression for $\Gamma_b$ in eq 27 agrees with the exact treatment (eqs A1-5 and A1-6) to better than 2%.[27] In the calculations that follow, the liquid-phase diffusion coefficient $D_l$ and its temperature dependence are obtained from Houghton.[28] At 291 K, $D_l = 2.01 \times 10^{-5}$ cm$^2$ s$^{-1}$ for both $NH_3$ and $NH_4^+$. Rate coefficients $k_f$ and $k_f'$ are obtained from Emerson et al.[29] and Eigen et al.[30] and are listed in Table 4 (Appendix 2).

**Gas-Phase Diffusion.** It was pointed out by Shi et al.[12] that gas-phase diffusive transport of a trace gas to a train of droplets has not been treated analytically. In fact, gas-phase diffusive transport does not lend itself to a straightforward analytical solution over the full range of Knudsen numbers even for a single stationary droplet. However, an empirical formulation of diffusive transport to a stationary droplet developed by Fuchs and Sutugin[31] has been shown to be in good agreement with measurements (see Widmann and Davis[32]).

Using the Fuchs−Sutugin formulation, Hanson et al.[33] extracted an expression for $\Gamma_{diff}$ as

$$\frac{1}{\Gamma_{diff}} = \frac{0.75 + 0.283K_n}{K_n(1 + K_n)} \quad (28)$$

Here, $K_n$ is the Knudsen numbers defined as $2\lambda/d_f$, where $\lambda$ is the gas-phase mean free path with $\lambda = 3D_g/\bar{c}$; $d_f$ is the effective diameter of the droplets for the diffusive process. Equation 28 is a more accurate treatment of gas-phase diffusion than was used in our earlier studies.[9] However, in the range of the earlier studies the two treatments are in close agreement.

Our early experiments, described in Worsnop et al.,[9] have shown that diffusive transport to the train of moving droplets, closely spaced (3−12 droplet diameters), is independent of droplet diameter but depends rather on the diameter of the droplet-forming orifice $d$ such that, in eq 28, $d_f = (1.9 \pm 0.1)d$. In other words, the measurements showed that as the diameter of the droplets was changed over a range of about a factor of 6, with other factors kept constant, the gas uptake per unit area (i.e., $\gamma_{meas}$) remained constant. Further, diffusive transport was adequately described by eq 28 with $d_f$ depending only on the orifice diameter as indicated. Therefore, $d_f$ is to be considered the effective diameter for the diffusive process.

Recently performed $NH_3$(g) uptake measurements on sulfuric acid droplets, described in the following companion paper, made it possible to perform studies of diffusive transport over a wide range of Knudsen numbers ($K_n$ = 0.05−4.5) with uptake coefficients ranging from 0.06 to 1.[8] The results of these measurements confirmed the earlier findings of Worsnop et al.[9] that diffusive transport to the train of moving droplets is independent of droplet diameter. The new more extensive studies yield $d_f = (2.0 \pm 0.1)d$. The studies also showed that, over the full range of Knudsen numbers ($K_n$ from 0.05−4.5) and mass accommodation coefficients ($\alpha$ from 0.01 to 1), gas-phase diffusive transport is in accord with the formulation of Fuchs and Sutugin.[31]

The diffusion coefficient $D_g$ (cm$^2$ s$^{-1}$) for $NH_3$ in the water vapor plus helium background gas is computed as shown in Worsnop et al:[9]

$$\frac{1}{D_g} = \frac{p_{H_2O}}{D_{NH_3-H_2O}} + \frac{p_{He}}{D_{NH_3-He}} \quad (29)$$

Here, $p$ is the partial pressure of the subscripted gas species, and $D_{NH_3-H_2O}$ and $D_{NH_3-He}$ are the binary gas-phase diffusion coefficients for species $NH_3$ in $H_2O$ and He, respectively.

Gas-phase diffusion coefficients for $NH_3$ are not available in the literature. However, they can be calculated by using the CHEMKIN computer program.[34] At 298 K $D_{NH_3-H_2O} = 0.215$ atm cm$^2$ s$^{-1}$, $D_{NH_3-He} = 0.901$ atm cm$^2$ s$^{-1}$, and $D_{NH_3-Ar} = 0.233$ atm cm$^2$ s$^{-1}$. Calculations show that those coefficients with rare gases vary as $T^{1.7}$, while $D_{NH_3-H_2O}$ varies as $T^{2.0}$. In the calculations of $D_g$, the average temperature between the droplet surface and the ambient gas was used. This way of treating the temperature gradient in the ambient gas is discussed in Worsnop et al.[9] It is also shown there that the effect of this gradient on the droplet temperature is negligible.

**Effect of $NH_3$ Uptake on pH.** As $NH_3$(g) enters the liquid, it diffuses into the bulk and via the reactions shown in eqs 19 and 20 it generates [$OH^-$] or consumes [$H^+$]. As a result, the pH of the liquid increases within the diffusion layer. Under the conditions of the droplet experiments, equilibrium is not attained, and the pH near the surface is time dependent.

The near surface pH is calculated using the Acuchem program as outlined in Appendix 2. The calculations show that for $NH_3$(g) densities in the range $10^{13}-2 \times 10^{14}$ cm$^{-3}$ used in our experiment, the pH is altered by the ammonia entering the liquid when the initial pH is set in the region between $pH_o = 2-10$. In what follows, unless otherwise stated, all pH values quoted have been adjusted for the effect of ammonia uptake.

## Experimental Section

Ammonia uptake studies on a millisecond time scale were conducted using a droplet train apparatus shown schematically in Figure 2 and described previously.[9] A fast-moving (1500−3000 cm/s), monodisperse spatially collimated train of aqueous droplets was passed through a 30 cm long longitudinal low pressure (6−20 Torr) flow tube which contains the gas-phase ammonia at a density in the range $10^{13}$ to $2 \times 10^{14}$ cm$^{-3}$ entrained in a flowing mixture of helium and water vapor. The flowing carrier gases are introduced at the entrance of the reactor. The flowing trace gas is introduced through one of three loop injectors located along the flow tube. By selecting the gas inlet port and the droplet velocity, the gas-droplet interaction time can be varied between 2 and 15 ms.

The stream of droplets is produced in a separate chamber by a vibrating orifice 70 $\mu$m in diameter which generates droplets in the range 150−300 $\mu$m in diameter, depending on the frequency of orifice vibration. The surface area of the droplets passing through the flow tube is changed in a stepwise fashion by changing the orifice driving frequency. The density of the trace gas is monitored with a quadrupole mass spectrometer. The uptake coefficient ($\gamma_{meas}$), as defined by eq 3, is calculated from the measured change ($\Delta n_g$) in trace gas signal via eq 30.

$$\gamma_{meas} = \frac{4F_g}{\bar{c}\Delta A} \ln \frac{n_g}{n_g'} \qquad (30)$$

Here $F_g$ is the carrier-gas volume rate of flow (cm$^3$ s$^{-1}$) through the system, $\Delta A = A_1 - A_2$ is the change in the total droplet surface area in contact with the trace gas, and $n_g$ and $n_g'$ are the trace gas densities at the outlet of the flow tube after exposure to droplets of area $A_2$ and $A_1$ respectively ($n_g = n_g' + \Delta n_g$).

The apparatus in these studies varies in one significant way from the previously described system. In the earlier studies the species in the mass spectrometer were ionized conventionally by electron impact. Since electrons ionize both water and ammonia, this method is not suitable for detecting a small amount of ammonia (mass 17) in the presence of a large amount of water. In the present experiments ammonia ions are produced by photoionization with ultraviolet light ($\lambda = 121.6$ nm) from a microwave discharge of 1 Torr hydrogen in helium. The light produced in this way selectively ionizes ammonia but not water vapor. Photoionization is performed between two sampling apertures of the differentially pumped vacuum system. Sampling in this lower pressure region rather than in the flow tube reduces significantly clustering of ammonia with water molecules.

An important aspect of the experimental technique is the careful control of all conditions within the apparatus. Water vapor pressure control is especially important because the temperature of the droplets is determined by the partial pressure of $H_2O$ in both the droplet generation chamber and in the flow tube.[9] The present experiments were done with the partial pressure of $H_2O$ in the reaction zone between 17.5 and 2.15 Torr, corresponding to temperatures between 20 and −10 °C, respectively. The lower temperatures, below 0 °C, are obtained by evaporatively cooling the droplets which are supercooled but not frozen.[9] Overall pressure balance in the flow tube is further checked by sequentially monitoring the concentration of a reference gas, in this case NO (which is likewise photoionized). Because NO is effectively insoluble in water, any change in NO concentration with droplet switching determines the "zero" of the system and is subtracted from observed changes in $NH_3$ trace gas concentration.

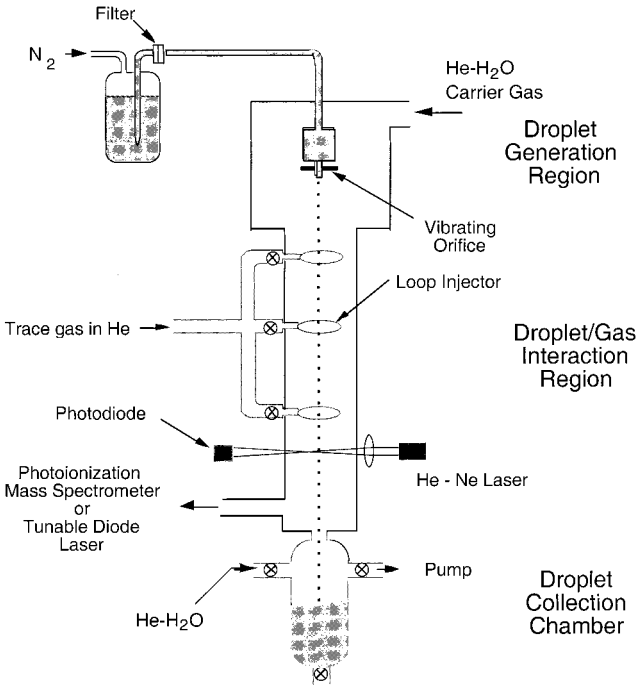


**Figure 2.** Schematic of droplet train flow reactor apparatus. Description is found in the text.

The reagent $NH_3$ (99.5%) and the reference gas NO (99.998%) were purchased from Matheson Gas Co. The species were diluted in helium and were used without further purification. In most experimental runs the density of ammonia in the flow tube was about $5 \times 10^{13}$ cm$^{-3}$. However, to test various aspects of the experiment, in specific experimental runs the density was varied from about $5 \times 10^{12}$ to $3 \times 10^{14}$ cm$^{-3}$. The density of NO was in the same range. The droplets were prepared with initial pH (designated as $pH_o$) in the range from 0 to 13. The low pH was set with sulfuric acid and the high pH with NaOH. As was discussed, ammonia molecules which enter the water alter the near-surface pH of the droplet via reactions shown in eqs 19 and 20, making it more basic. This effect which is a function of $NH_3$(g) density is taken into account as described in Appendix 2.

## Results and Analysis

**Uptake Measurements.** Uptake measurements were performed as a function of droplet area, gas flow rate, gas-droplet contact time, droplet temperature and droplet pH. As an example of the measurements, we show in Figure 3 a plot of $\ln(n_g/n_g')$ for $NH_3$ as a function of $\bar{c}\Delta A/4F_g$ at 291 K and pH = 0.3. Here $\bar{c}\Delta A/4F_g$ was varied by changing the gas flow rate and the droplet surface area ($\Delta A$). Each point is the average of at least 10 area change cycles and the error bars represent one standard

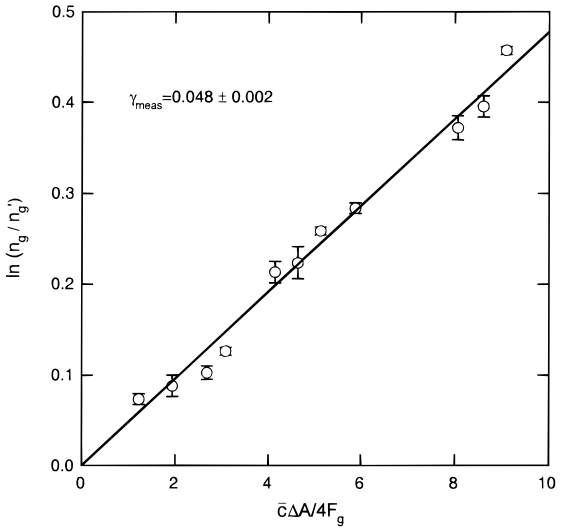


**Figure 3.** Plot of $\ln(n_g/n_g')$ as a function of $\bar{c}\Delta A/4F_g$ for ammonia. Droplet pH = 0.3, droplet temperature $T_d$ = 291 K. Line is the least-squares fit to the data. Slope of the line is $\gamma_{meas.}$

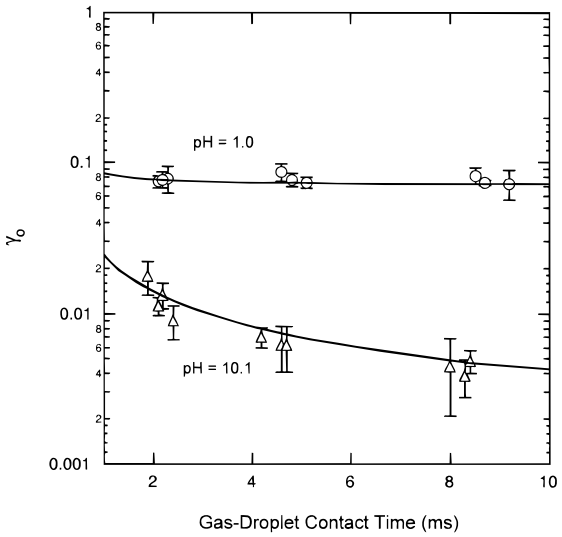


**Figure 4.** Ammonia uptake coefficient $\gamma_0$ as a function of gas−droplet contact time. Droplet pH = 1 and 10.1, droplet temperature $T_d$ = 291 K, and $NH_3$ density = $4 \times 10^{13}$ cm$^{-3}$. The solid lines are calculations based on eqs 4 and 27, and the circuit analogue of Figure 1a.

deviation from the mean in the experimental $\Delta n/n$ value. As is evident in eq 30, the slope of the plot in Figure 3 yields a value of $\gamma_{meas}$. For this data set, $\gamma_{meas} = 0.048 \pm 0.002$. Such plots were obtained for the full range of uptake studies. In these studies the uptake signal $\Delta n/n$ varied typically from 2% to 30%. The linearity of the plots over an order of magnitude in the uptake signal validates the measurement procedure.

**Uptake as a Function of Gas−Liquid Interaction Time.** In Figure 4 we show the gas-transport-free uptake coefficient $\gamma_0$ as a function of gas-droplet contact time for pH = 1.0 and pH = 10.1 at 291 K. Gas diffusion is taken into account via eqs 4 and 28. The gas-phase ammonia density in these studies was $4 \times 10^{13}$ cm$^{-3}$. At pH 1, within the accuracy of our data, the uptake coefficient is independent of gas−liquid contact time on our experimental time scale. On the other hand, the pH 10.1 uptake exhibits a clear time dependence.

The time dependence of $\gamma_o$ is governed by solubility. Referring to Figure 1a and eq 27, time dependence of the uptake will be evident if $\Gamma_{sol}^{-1} \geq \alpha^{-1}$. At pH = 10, $\Gamma_{sol}^{-1} \sim 100$ and $\Gamma_{sol} \sim \Gamma_b$. As will be shown, $\alpha^{-1}$ is on the order 10. Therefore,

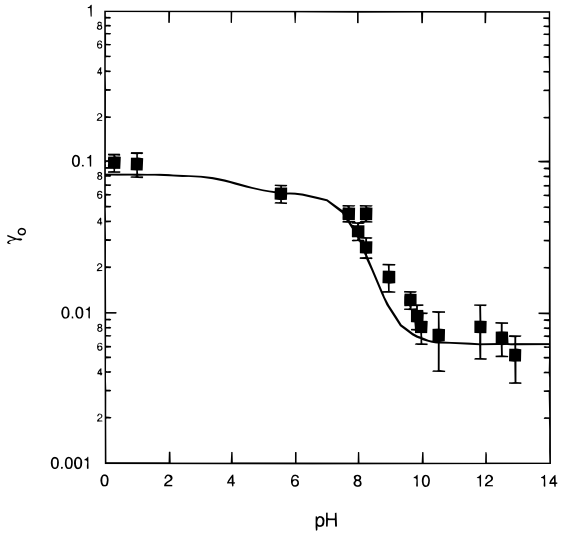


**Figure 5.** Ammonia uptake coefficient $\gamma_0$ as a function of pH. Droplet temperature $T_d$ = 291 K, gas-droplet contact time $t$ = 5 ms and ammonia density ranging from $1 \times 10^{13}$ to $2 \times 10^{14}$ cm$^{-3}$. The solid line is a calculation based on the model discussed in the text.

here the uptake is dominated by $\Gamma_{sol}^{-1}$ which is time dependent. On the other hand, at pH = 1, on the time scale of 10 ms $\Gamma_b^{-1}$ is less than 0.03. Therefore, in this region, $\Gamma_b^{-1}$, is negligible compared to $\alpha^{-1}$, and the uptake is governed by mass accommodation. Solid lines in Figure 4 are model calculations based on eq 4 and the circuit analogue of Figure 1c, using values of H and $\alpha$ obtained from the measurements. The modeling includes the effect of a surface complex (via $\Gamma_s$), as will be discussed.

**Uptake as a Function of pH.** The gas-phase diffusion corrected uptake coefficient $\gamma_0$ as a function of pH is shown in Figure 5. The data were obtained at $T$ = 291 K, and a gas liquid interaction time of 5 ms. The gas phase $NH_3$ densities in this set of data range from $1 \times 10^{13}$ to $2 \times 10^{14}$ cm$^{-3}$. For each data point in the figure, the actual pH, as affected by the ammonia uptake, is calculated as shown in Appendix 2. The solid line in the figure represents calculated values of $\gamma_o$ based on the previously discussed model.

The nature of the uptake process is conveniently interpreted from data at the two extremes of pH. As mentioned, at low pH, $\Gamma_b$ is large and therefore if surface effects are relatively small, then in this region the uptake is governed by the mass accommodation coefficient $\alpha$. That is, in this region $\gamma_0 \cong \alpha$. At high pH, $\Gamma_{sol}$ is small compared to $\alpha$ and uptake is dominated by $\Gamma_{sol}$ and surface effects, if any.

In the midrange, going from pH 10 to 7, the uptake rises due to increasing solubility of $NH_4^+$ (reactions in eqs 19 and 20), here $\gamma_o$ is determined by $\Gamma_{sol}$ ($NH_4^+$). The model calculation shown in Figure 5 shows leveling of $\gamma_o$ in two regions; around pH 5 and then around pH 1. The experimental data are in accord with this trend. The plateau around pH 5 is due to the reaction rate of $NH_3$ with $H_2O$ which limits the uptake process via $\Gamma_{rxn}^{-1}$. The slow rise between pH 5 and 3 reflects an increase in $\Gamma_{rxn}$ due to $NH_3$ reaction with $H^+$ (eq 20). In this region, $\Gamma_b = \Gamma_{rxn}$. As pH decreases further, $\Gamma_{rxn}$ continues to increase and the uptake becomes limited by the mass accommodation $\alpha$. (See eq 4.)

**Mass Accommodation Coefficient.** The mass accommodation coefficients obtained from the uptake measurements at pH = 1 are shown as a function of temperature in Figure 6. The figure also includes the measurements of Bongartz et al.[7] obtained at 298 K and Ponche et al.[6] at 290 K. As can be seen, their results are in good agreement with our data.

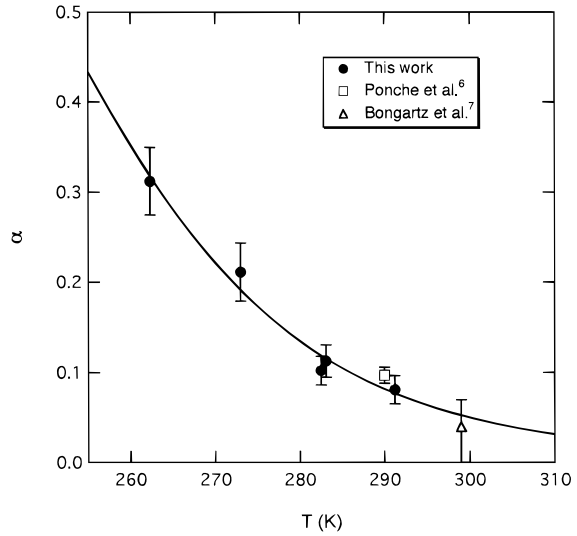


**Figure 6.** Mass accommodation coefficient α for ammonia as a function of temperature. Solid line is a calculation based on eq 31 with $\Delta G_{obs}$ obtained from Figure 7.

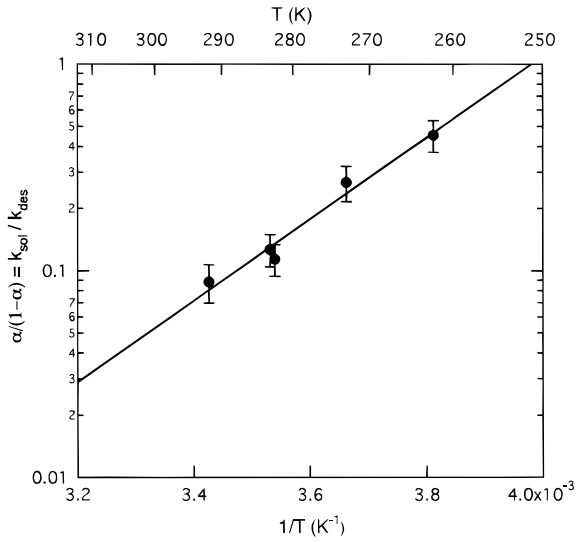


**Figure 7.** Semilog plot of α/(1-α) versus 1/*T* for ammonia (see eq 31). The solid line is the least-squares fit to the data, providing values for $\Delta H_{obs} = -9.02 \pm 0.8$ kcal/mol and $\Delta S_{obs} = -35.9 \pm 2.9$ cal/(mol K).

It was shown by Jayne et al.[22] that the mass accommodation coefficient can be expressed as

$$\frac{\alpha}{1-\alpha} = \frac{k_{sol}}{k_{des}} = \exp\left(\frac{-\Delta G_{obs}}{RT}\right) \qquad (31)$$

The parameter $\Delta G_{obs}$ is the Gibbs energy of the transition state between gas phase and aqueous phase solvation. The mass accommodation measurements are then expressed in terms of eq 31 by plotting $\ln(\alpha/1-\alpha)$ as a function of 1/*T*. The slope of such a plot is $-\Delta H_{obs}/R$ and the intercept is $\Delta S_{obs}/R$. Such a plot for ammonia but on a log scale is shown in Figure 7 and yields $\Delta H_{obs} = -9.02 \pm 0.8$ kcal/mol and $\Delta S_{obs} = -35.9 \pm 2.9$ cal/(mol K). The solid line in Figure 6 is a plot of eq 31 with these parameters.

**Uptake at High pH: Ammonia Surface Complex.** As stated earlier, at high pH, $\Gamma_{sol} \sim \Gamma_b$. Therefore, in the absence of surface effects, $\gamma_o^{-1} = \Gamma_{sol}^{-1} + \alpha^{-1}$ and one would expect a plot of $1/\gamma_o$ as a function of $t^{1/2}$ to be a straight line with positive intercept of $\alpha^{-1}$. (See eqs 4, 23 and 27.) Such a plot of the uptake coefficient at pH = 13 and $T = 291$ K as a function of $t^{1/2}$ is shown in Figure 8 as a solid line. It is immediately evident that the measurements are not in accord with eq 4. The best fit straight line plot leads to a negative intercept. Similar results are obtained at the three other temperatures studied; 283, 273, and 264 K. The dashed line is the best straight line fit to bulk phase parameters with a forced nonnegative intercept. Although this line does skirt the error bars of the data, still we consider this fit inadequate.

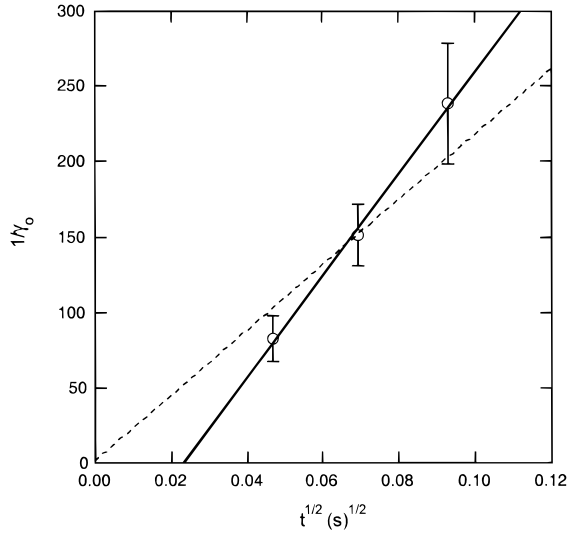


**Figure 8.** $1/\gamma_0$ for ammonia at pH = 13 and $T = 291$ K as a function of $t^{1/2}$. Solid line is the least-squares fit based on eqs 4, 27, and 23, negative intercept indicative of surface complex. Dashed line is the best fit with positive intercept which assumes no surface complex (see text).

To interpret the ammonia uptake data in Figure 8, we turn to our earlier $SO_2$ uptake studies.[16] Qualitatively the uptake of ammonia at high pH is expected to be similar to that of $SO_2$ at low pH. The uptake of $SO_2$, however, is simpler, since its physical Henry's law constant is small ($H = 1.6$ M atm$^{-1}$ at 291 K) so that $\gamma_{meas}$ as calculated from eq 4 is $\sim 10^{-4}$, too small to be measured with the droplet apparatus. In fact, in the $SO_2$ experiment we did observe a measurable uptake with the notable feature that the product of the uptake coefficient and the gas−liquid interaction time is a constant (i.e., $\gamma_{meas}\, t = C$).

A simple way to explain this observed behavior is to assume that $SO_2$ forms a surface complex at the gas liquid interface, most likely in an ionic form $H^+-HSO_3^-$. That is, the collision rate of gas phase species with the droplet surface is sufficiently high, such that a species surface layer can be established in a fraction of a millisecond which is faster than the experimental gas liquid interaction time. Therefore, as stated in the modeling section of this paper, on the time scale of the uptake experiments, this surface complex is in equilibrium with the gas-phase species and provides a one-time, time-independent contribution to the uptake flux.

The physical Henry's law constant of ammonia is about 30 times higher than that of $SO_2$. As a result, uptake due to the solvated ammonia is measurable even at the high pH end of our studies. Therefore, the clear surface complex-type behavior observed for $SO_2$ is not unambiguously evident in the $NH_3$ uptake data. However, it does seem reasonable to assume that the deviation of the high pH data from the uptake based on bulk phase parameters shown in Figure 8 is due to a surface complex.

In past uptake studies with acetaldehyde[35] and formaldehyde,[10] we also observed deviations from bulk phase kinetics,

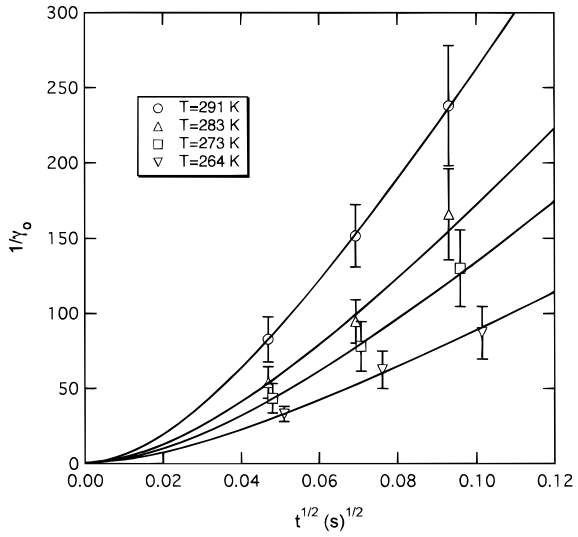


**Figure 9.** $1/\gamma_0$ for ammonia as a function of $t^{1/2}$. Lines are nonlinear model fits taking into account solubility and a surface complex. Circles are same data shown in Figure 8.

suggesting the presence of a surface complex. What ties the molecules forming a surface complex together is the possibility of these species to form an ionic complex. (Acetaldehyde can undergo aldol condensation forming the enolate ion, and formaldehyde at high acidity is thought to form a protonated surface species.)

Ammonia likewise falls into the ion-forming category with a possible $NH_4^+-OH^-$ surface complex formation. On the other hand, the uptake of acetone which does not form an ionic complex and has a Henry's law constant (47.7 M atm$^{-1}$ at 291 K) comparable to $NH_3$ shows no deviation from bulk liquid-phase kinetics.[36]

As indicated in Figure 8 by the dashed line skirting the error bar extremities of the data, a fit consistent with bulk phase kinetics can be obtained. However, we believe that the deviation from bulk phase kinetics shown by the best fit line is real. This is based on the observations that the trend shown in Figure 8 by the best fit line is also evident at the other three temperatures studied. Further, the uptake data at low pH show no time dependence, confirming that the time dependent deviation from bulk kinetics shown in Figure 8 is due to a surface complex as represented by eq 10 via eq 16. We will therefore analyze the data in terms of a surface complex.

The surface uptake coefficient $\Gamma_s^{cx}$, due to the formation of complex at the surface is given by eq 16, as

$$\Gamma_s^{cx} = 4/(\bar{c}t)\, n_s^{cx}/n_g = 4/(\bar{c}t)\, A^{cx}_{eq}$$

Here $n_s^{cx}$ is ammonia surface species density (cm$^{-2}$) responsible for the additional uptake. The gas-phase diffusion-free uptake coefficient $\gamma_0$ is obtained from analysis based in Figure 1b with $\Gamma_s^{cx}$ as defined by eq 16.

The high pH uptake results at four temperatures studied were individually fitted to the surface model discussed, with Henry's law constant $H$, and $A^{cx}_{eq}$ as the two parameters to be fitted. The experimental results and the model fits are shown in Figure 9. The gas-phase $NH_3$ density in these experiments was about $10^{14}$ cm$^{-3}$.

The parameter $A^{cx}_{eq}$ obtained from the fits for ammonia at the four temperatures and the previously measured $A^{cx}_{eq}$ values for sulfur dioxide, formaldehyde, and acetaldehyde surface species are listed in Table 1.[10,16,35] As shown in the table, $A^{cx}_{eq}$ for ammonia is somewhat higher but on the same order as that

**TABLE 1: $A^{cx}_{eq}$ for Different Molecules**

| temperature (K) | $A^{cx}_{eq}$ (cm) for $NH_3$ | $A^{cx}_{eq}$ (cm) for $SO_2$ | $A^{cx}_{eq}$ (cm) for formaldehyde | $A^{cx}_{eq}$ (cm) for acetaldehyde |
|---|---|---|---|---|
| 263 | 0.69 | | 0.12 | |
| 267 | | | | 0.29 |
| 273 | 0.53 | | | |
| 283 | 0.42 | 0.13 | | |
| 291 | 0.27 | | | |

**TABLE 2: Henry's Law Constant at 293 and 273 K**

| | $H$ (M atm$^{-1}$) at 293 K | $H$ (M atm$^{-1}$) at 273 K |
|---|---|---|
| this work | 34.2 | 76.3 |
| Sorina et al.[39] [a] | 40.5 | 96.8 |
| Sherwood[40] | 30.1 | 45.7 |
| Clegg and Brimblecombe[42] | 77.7 | 220.4 |
| Hales and Drewes[41] | 93.9 | 236.0 |

[a] Extrapolated from higher temperature.

of the other three molecules. As is evident, $A^{cx}_{eq}$ exhibits a negative temperature dependence. Using the values of $A^{cx}_{eq}$ listed in Table 1, the surface density $n_s^{cx}$ can be computed. For ammonia, with $n_g = 10^{14}$ cm$^{-3}$, $n_s^{cx}$ ranges from $2.6 \times 10^{13}$ cm$^{-2}$ at 291 K to $7.8 \times 10^{13}$ cm$^{-2}$ at 264 K.

Taking into account surface saturation, $n_s^{cx}$ can be expressed as[37]

$$n_s^{cx} = \frac{N_{max}}{1 + \dfrac{N_{max}}{A^{cx}_{eq} n_g}} \tag{32}$$

where $N_{max}$ is the maximum number of adsorbed molecules on the surface (cm$^{-2}$) (i.e., the number of molecules required to form a monolayer).

The surface species density $n_s^{cx}$ can also be expressed in terms of the aqueous ammonia concentration by using the equilibrium relation between gas- and aqueous-phase ammonia. That is,

$$n_s^{cx} = \frac{N_{max}}{1 + \dfrac{b}{X}} \tag{33a}$$

where

$$b = N_{max} HRTM_{H_2O}/(A^{cx}_{eq} N_A \rho) \tag{33b}$$

$X$ is the mole fraction of solvated ammonia, which under our experimental conditions at 291 K is $2.6 \times 10^{-6}$. $N_A$ is Avogadro's number, $\rho$ is the $H_2O$ density in g/cm$^3$, and $M_{H_2O}$ is the molecular weight of water. Equation 33a is in the form of the Langumir expression as used by Castro et al.,[37] and Karpovich and Ray.[38] Here $b$ is expressed in terms of $\Delta G_{ads}$, the free energy of the surface species with respect to the solvated species, $b = \exp(\Delta G_{ads}/RT)$. Assuming a typical value of $N_{max} = 1 \times 10^{14}$ cm$^{-2}$, our experimental data yield $\Delta H_{ads}$ and $\Delta S_{ads}$ as $-2.9 \pm 0.7$ kcal/mol and $-13.7 \pm 2.6$ cal/(mol K), respectively. At 291 K, $\Delta G_{ads}$, for ammonia is $-6.7$ kcal/mol.

**Henry's Law Constants.** The Henry's law constants for ammonia obtained from our measurements along with literature values for this parameter are shown in Table 2 and are plotted in Figure 10 as a function of $T^{-1}$. Our solubility data analysis includes the salting-out effect of NaOH which is used to set the base pH of the aqueous droplets. This effect is less than 10%. The line in the figure is the least-squares log $H$ vs $1/T$ fit to the present data and the data of Sorina[39] which were obtained

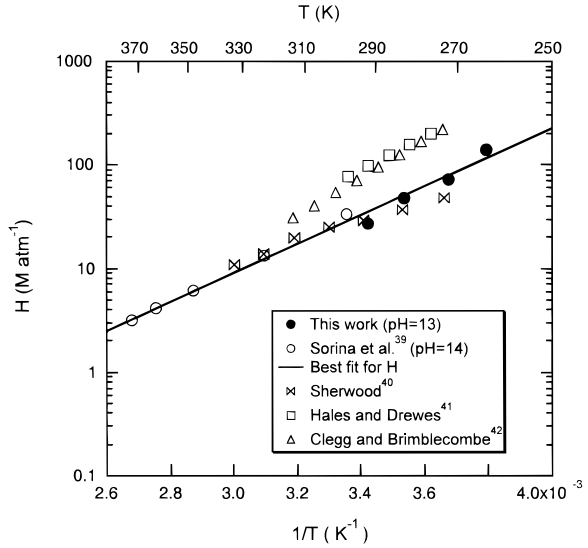


**Figure 10.** Henry's law constants for ammonia as a function of $T^{-1}$. Line is the least-squares semilogarithm fit to our data and the data of Sorina et al.

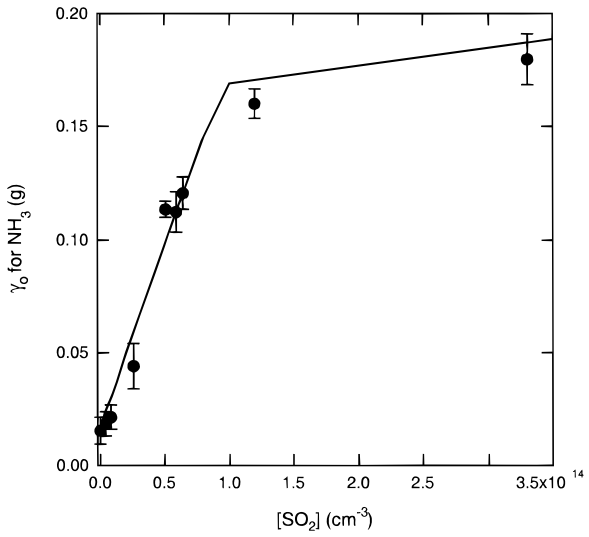


**Figure 11.** Ammonia uptake coefficient $\gamma_0$ in $NH_3/SO_2$ codeposition studies as a function of gas-phase $SO_2$ density. Aqueous surface initially at $pH_o = 4$, $NH_3$ density $= 5 \times 10^{13}$ cm$^{-3}$, $T = 273$K. Line is a numerical calculation described in Appendix 2.

under conditions similar to ours; that is at high pH (our measurements were at pH = 13, Sorina's at pH 14). The data of Sherwood[40] were obtained at a high concentration of aqueous $NH_3$. The measurements of Hales and Drewes[41] were obtained at pH = 4 and 7 and those of Clegg and Brimblecombe[42] at pH = 7. (See Discussion.) The Henry's law constant (M atm$^{-1}$) over the temperature range of 264−350 K derived from the fit is expressed by

$$\log H = -3.221 + 1396/T \qquad (34)$$

Clearly, our data are in agreement with the measurements of Sorina[39] but deviate from the data of Hales and Drewes,[41] and Clegg and Brimblecombe.[42] As will be discussed, we believe that the straight line fit is currently the best representation of the ammonia Henry's law constant.

**Codeposition Studies.** The uptake of $NH_3$ was also studied in co-deposition experiments where a known amount of $SO_2$ gas was added to the flow of $NH_3$ gas. The ammonia uptake coefficient $\gamma_0$ in such a $NH_3/SO_2$ codeposition study is shown in Figure 11. The initial pH of the droplet was set at $pH_o = 4$, the temperature was 273K and the $NH_3$ density was held constant at $5 \times 10^{13}$ cm$^{-3}$. Qualitatively the results in Figure 11 are easily understood. In the absence of $SO_2$, at an $NH_3$ density of $5 \times 10^{13}$ cm$^{-3}$, the near surface pH of the droplet shifts to pH = 9.2 because of the $OH^-$ produced via eqs 19 and 20. In this region the solubility of ammonia is low and the uptake coefficient $\gamma_0$ has a relatively small value of 0.015. As $SO_2$ is added, the $H^+$ produced in the reaction $SO_2 + H_2O \rightarrow H^+ + HSO_3^-$ acidifies the solution increasing the effective ammonia solubility and hence its uptake. The ammonia uptake rises with $SO_2$ density until the uptake plateau with pH is reached, (corresponding to the plateau observed in Figure 5). The solid line in the figure is the result of model calculations which take into account the $SO_2$ acidification (see Appendix 2). As is evident the measurements are in accord with these calculations. A reverse co-deposition study in which the $SO_2$ density was held constant and the $NH_3$ density was varied was also conducted and was likewise found to be in accord with calculations.

## Discussion

The ammonia uptake data lend themselves to comparison with the earlier results obtained for $SO_2$.[16] The most evident feature in the data for both species is the dependence of the uptake on pH. At high pH ammonia uptake is governed principally by solubility and surface species uptake. As pH decreases the effective Henry's law constant increases and the uptake rises correspondingly tending toward a plateau limited by the mass accommodation coefficient. Since $SO_2$ is an acid, its uptake as a function of pH exhibits the opposite pattern.

**Mass Accommodation.** The mass accommodation coefficient for ammonia increases from 0.08 at 290 K to 0.35 at 260 K. This negative temperature dependence is consistent with the nucleation model which was formulated to explain the uptake of a large number of previously studied species. The Gibbs parameters for ammonia that is, $\Delta H_{obs} = -9.02$ kcal/mol and $\Delta S_{obs} = -35.9$ cal/(mol K) are similar to those measured for alcohols.[43,23]

**Surface Complex.** We certainly want to understand the nature of the surface complex observed in our experiment. Specifically, we want to know the connection (if any) between the measured surface complex and the Gibbs surface excess ($\Gamma'$). The Gibbs surface excess ($\Gamma'$) is calculated from surface tension ($\sigma$) data (see, for example, Lewis et al.,[44] eq 29.20). That is,

$$\Gamma' = \frac{-X}{RT}\left(\frac{\partial \sigma}{\partial X}\right) \qquad (35)$$

Here, as before, $X$ is $NH_3$ aqueous phase mole fraction. Equation 35 yields the surface excess concentration rather than the total surface concentration; however, under our experimental conditions, the two are nearly equal.[12]

Using the available $NH_3-H_2O$ surface tension data [45] at 291 K with $n_g = 1 \times 10^{14}$ cm$^{-3}$, the surface excess $\Gamma' = 1.4 \times 10^{10}$ molecules cm$^{-2}$, and the free energy of the Gibbs surface excess $\Delta G_s'$ is −2.1 kcal/mol. Recent time-dependent surface tension measurements with high concentration $NH_3$ solutions performed by Donaldson[46] are in accord with eq 35.

As is evident, the surface species observed in our studies cannot be associated with the thermodynamic Gibbs surface excess of eq 35. The value of $n_s^{cx}$ is about 3 orders of magnitude larger than $\Gamma'$. At comparable $NH_3$(g) densities, $n_s^{cx} \sim 2 \times 10^{13}$ compared to $\Gamma' \sim 1 \times 10^{10}$ molecules cm$^{-2}$. Correspondingly, at 291 K, $\Delta G_{ads} = -6.7$ kcal/mol compared to $\Delta G_s' = -2.1$ kcal/mol. We note that the $SO_2$ surface complex measured in

previous uptake studies[16] was likewise about three orders magnitude higher than the Gibbs surface excess.

Recently, Simonelli et al.[47] used a "sum frequency generation" technique to probe the interface of aqueous ammonia solutions. The spectrum confirmed the existence of a surface complex. However, the qualitative nature of the data precludes identification of the surface species with Gibbs surface excess or the surface species observed in our experiments. At this point, the connection of surface species observed in our measurement to Gibbs surface excess or to the mass accommodation process is not evident. (See Discussion in Shi et al.[12])

**Henry's Law Constants.** As is evident from the data in Table 2 and Figure 10, there are significant differences in the values for the ammonia Henry's law constants found in the literature. The values of H fall into two groups: Those of Hales and Drewes,[41] and Clegg and Brimblecombe[42] are higher than the measurements of Sorina,[39] and Sherwood.[40] The present study yields *H*-values in agreement with those of Sorina and Sherwood.

There is one significant difference between the way the two groupings were measured. The higher *H* values were measured with solutions at relatively low pH. Clegg and Brimblecombe's values were obtained by a reanalysis of the calculation of Chen[48] which were in turn based on experimental data of Van Krevelen[49] performed with buffered solutions at pH = 7. Hales and Drewes' data were obtained at pH = 4 and 7. On the other hand, the lower values of H were all obtained at high pH (Sorina at pH = 14, Sherwood at pH = 12.6, present study at pH = 13). One might argue that the higher pH measurements tend to be more accurate since in that region the hydrolysis process (eq 19) does not have a significant effect on the ammonia equilibrium. Therefore, at this point we recommend the lower value of H as expressed in eq 34.

**Codeposition.** One might expect that the presence of a surface complex such as was observed in the $SO_2$ and $NH_3$ uptake studies would have some chemical consequences. So far this has not been observed. Neither the codeposition studies presented in this work nor earlier studies of $SO_2$ uptake in the presence of hydrogen peroxide[50] show significant deviations from uptake predicted by bulk liquid-phase chemistry.

**Atmospheric Implications.** For compounds which are highly soluble, mass transport to atmospheric aerosols is a function of the mass accommodation coefficient $\alpha$ and the gas-phase diffusion uptake coefficient ($\Gamma_{diff}$). The parameter $\alpha$ is rate limiting when $\alpha < \Gamma_{diff}$. The mass accommodation coefficient for $NH_3$ was measured to be in the range 0.08−0.35 as the temperature decreases from 290 to 260 K. The magnitude of $\Gamma_{diff}$ depends on the size of the droplet. At 400 Torr (characteristic of the upper troposphere) $\Gamma_{diff}$ is larger than 0.1 for aerosols with diameters less than 1 $\mu$m. A significant fraction of tropospheric aerosols is in this size range. Therefore, realistic modeling of ammonia−aerosol interactions should utilize accurate values of the mass accommodation coefficient.

Finally, we compare the amount of surface $NH_3$ (as observed in this work) to the ammonia content in the bulk liquid for an atmospheric aqueous droplet of diameter d. The surface to bulk content ratio is given by Jayne et al.[16]

$$\text{surface to bulk } (NH_3) = \frac{6\pi d^2}{\pi d^3}\frac{A^{cx}_{eq}}{H^*RT} \qquad (36)$$

For a 10 $\mu$m cloud droplet at pH 6, in equilibrium with gas-phase $NH_3$, the ratio of ammonia on the surface compared to the bulk is small, about $10^{-3}$. On the other hand, for a 1 $\mu$m droplet at pH 8 (such as might be the case for a deliquescent sea-salt aerosol), the surface-to-bulk ratio of ammonia is about 1. In this case surface chemistry, specifically photochemistry of the surface complex, may be important. This possible effect will be investigated in future studies.

## Appendix 1

**Exact Solutions for the Gas Uptake Processes.** *1. Uptake Limited by Solubility.* When the gas uptake is governed solely by mass accommodation and solubility, the results of Danckwerts[13] yield the expression

$$\gamma_o(t) = \frac{\int_0^t \alpha\ \mathrm{erfc}(gt'^{1/2})\ \exp(g^2t')\ \mathrm{d}t'}{t} \qquad (A1\text{-}1)$$

where $t$ is the gas−liquid interaction time,

$$g = \frac{\alpha\bar{c}}{4HRTD_1^{1/2}} \qquad (A1\text{-}2)$$

and $H$ and $D_l$ are species Henry's law constant and liquid-phase diffusion coefficient.

The exact solution to this integral can be found in Crank[51] yielding

$$\gamma_o(t) = \frac{\alpha}{g^2t}\left[\mathrm{erfc}(g\sqrt{t})\exp(g^2t) + 2g\sqrt{\frac{t}{\pi}} - 1\right] \qquad (A1\text{-}3)$$

The resistor model (eqs 4 and 27) is in agreement with eq A1-3 to better than 6%.[27]

*2. Uptake Limited by Irreversible Reaction and Solubility.* When the gas uptake is governed by mass accommodation, solubility, and irreversible chemical reactions, the work of Danckwerts[13] yields

$$\gamma_o(t) = \left\{\int_0^t \frac{\alpha}{g^2 - k_1}[g\sqrt{k_1}\ \mathrm{erf}(\sqrt{k_1t'}) + g^2\mathrm{erfc}(g\sqrt{t'})\ \exp\ (g^2t' - k_1t') - k_1]\ \mathrm{d}t'\right\}\Big/ t \qquad (A1\text{-}4)$$

Here $g$ is as defined in eq A1-2; $k_1$ is the forward pseudo-first-order rate coefficient.

For the $NH_3$ experiments, on the millisecond time scale of the droplet apparatus, $k_1t$ is greater than $10^3$, and the resistor model (eqs 4 and 27) is in agreement with eq A1-4 to better than 2%.[27]

*3. Uptake Limited by Reversible Reaction and Solubility.* The capacity of aqueous solutions to contain ammonia species increases with acidity. (See reactions shown in eqs 19 and 20.) The effect on $NH_3$ uptake of increased capacity is expressed by Danckwerts[14] in terms of an enhancement factor $E$ as

$$\Gamma_b = E\,\Gamma_{sol} \qquad (A1\text{-}5)$$

where $\Gamma_b$ and $\Gamma_{sol}$ are as defined in eqs 27 and 23, respectively.

In the case where both forward and backward reactions are first order, Sherwood and Pigford[15] provide an analytic expression for enhancement factor $E$ as:

$$E = (1+K)\left\{1 + \frac{K^2}{K^2-1}\frac{\sqrt{\pi}}{2a}\exp(a^2)[\mathrm{erf}(Ka) - \mathrm{erf}(a)] - \frac{K}{2a}\sqrt{\frac{\pi}{K^2-1}}\mathrm{erf}(a\sqrt{K^2-1})\right\} \qquad (A1\text{-}6)$$

Here for ammonia $K = K_b/[OH^-]$, $k_1$ is as defined in eq 26, and $a = \sqrt{k_1 t/[K(K-1)]}$. In their original equation (eq 389 of Sherwood and Pigford[15]), $E$ is designated as $f(K,k_1t)$. We note that Danckwerts[14] made a transcription error in his use of the Sherwood and Pigford results.[15]

Under the conditions of the $NH_3$ studies, the resistor model (eq 27) is in agreement with eq A1-6 to better than 2%.[27]

## Appendix 2

**1. Near-Surface pH.** To obtain the time-resolved surface pH, a solution is required for the differential equations that simultaneously take into account chemical reaction, liquid-phase diffusion, and mass transport at the interface. The general equation for the concentration $C_i$ of species ($NH_3$(aq), $NH_4^+$, $H^+$, $OH^-$) in the liquid phase is

$$\frac{\partial C_i}{\partial t} = D_i \frac{\partial^2 C_i}{\partial x^2} - k_i C_i \qquad \text{(A2-1)}$$

Here, $D_i$ is the species diffusion coefficient in the liquid, $k_i$ is the pseudo-first-order reaction rate in the bulk liquid for the $i$th species. A numerical solution for the differential equations is conveniently implemented using the *Acuchem* program.[52] Our strategy in using this program to simulate species reacting and diffusing into the liquid is to divide the liquid into bins of discrete thickness going from the surface into the liquid. The program can only handle a maximum of 99 species and 200 reactions. Therefore, we limit our treatment of the liquid to twice the diffusive depth ($Dt^{1/2}$) so that we can obtain a solution within the confines of the program. This layer is divided into 15 bins of equal size ($\Delta x$) with the species in each bin uniformly distributed. (The number of bins was varied to confirm that 15 bins provided an adequate resolution.) The droplet diameter in our experiments is in the range 150−300 $\mu$m. This is large compared to the diffusion depth of about 3 $\mu$m. Therefore, the droplet surface can be treated as a plane.

Using the basic definition of differentials and assuming that species can diffuse only to adjacent ($J-1$) and ($J+1$) bins, the diffusion term, (first term on the right-hand side of eq A2-1) can be approximated as

$$D_i \frac{\partial^2 C_i(J)}{\partial x^2} = \frac{D_i}{\Delta x^2}(C_i(J+1) + C_i(J-1) - 2C_i(J)) \qquad \text{(A2-2)}$$

Equation (A2-1) is then simplified to

$$\frac{\partial^2 C_i(J)}{\partial t} = \frac{D_i}{\Delta x^2}(C_i(J+1) + C_i(J-1) - 2C_i(J)) - k_i C_i(J) \qquad \text{(A2-3)}$$

Within the *Acuchem* computer program, the diffusion rate $D_i/\Delta x^2$ is treated simply as another "reaction" rate. The liquid-phase diffusion coefficient $D_i$ is obtained from Houghton.[28] As an example, the $SO_2$ diffusion coefficient at 290 K is $9.5 \times 10^{-6}$ cm$^2$/s. All parameters used in the calculation are listed in Tables 3 and 4.

The calculated surface pH values for $[NH_3(g)] = 1 \times 10^{14}$ cm$^{-3}$, at the gas−liquid interface (bin no. 1), are shown in Figure 12. The results are displayed as a function of $pH_o$. The solid line is the numerical solution of differential equations for typical experimental gas-liquid contact time of 5 ms. The dashed line is an equilibrium calculation based on charge balance, which can be found in the thesis of Shi.[27] In Figure 12, we also show numerical model calculation for gas liquid interaction time of 300 s (circles). As expected, at this relatively long gas−liquid interaction, equilibrium is approached and the numerical calculation yields results in accord with the equilibrium condition.

It is evident that for $pH_o$ less than about 4, equilibrium between gas phase $NH_3$ and the liquid-phase species is not attained on the millisecond time scale. For pH < 2, the initial $[H^+]$ concentration is sufficiently large so that the additional $OH^-$ generated by $NH_3$ does not affect pH. In the region of pH > 4, equilibrium is established rapidly and the surface pH obtained from numerical modeling is about the same as predicted by equilibrium calculations.

**TABLE 3: Parameters Used in the Calculations of Uptake Coefficient and Surface pH**

| | expression[a] | reference |
|---|---|---|
| $H$ ($NH_3$) | $\exp(-7.44 + 3214.4/T)$ | this work |
| $H$ ($SO_2$) | $\exp(-10.41 + 3168.6/T)$ | ref 53 |
| $K_b$ ($NH_3$) | $\exp(16.97 - 4411.1/T - 0.044T)$ | ref 54 |
| $K_a$ ($SO_2$) | $\exp(-10.91 + 1964.1/T)$ | ref 53 |
| $K_w$ | $\exp(-23.6 + 1550.1/T - 1.229 \times 10^6/T^2)$ | *b* |

[a] Concentrations is in mol/l; unit for H is M atm$^{-1}$. [b] Fitted to data in CRC handbook[55].

**TABLE 4: Reaction Rate Coefficients Used in Numerical Calculations[a]**

| reaction | rate coefficient | ref |
|---|---|---|
| 1. $NH_3(g) \rightarrow NH_3$ (aq) | $\bar{c}\alpha/(4\Delta x)1.66 \times 10^{-21}$, s$^{-1}$ | this work |
| 2. $NH_3(aq) \rightarrow NH_3$ (g) | $\bar{c}\alpha/(4\Delta x H_{NH_3} RT)$, s$^{-1}$ | this work |
| 3. $NH_3(aq) + H_2O \rightarrow NH_4^+ + OH^-$ | $5 \times 10^5$, s$^{-1}$ | ref 56 |
| 4. $NH_4^+ + OH^- \rightarrow NH_3(aq) + H_2O$ | $3 \times 10^{10}$, M$^{-1}$ s$^{-1}$ | ref 56 |
| 5. $NH_3(aq) + H^+ \rightarrow NH_4^+$ | $4.3 \times 10^{10}$, M$^{-1}$ s$^{-1}$ | ref 29 |
| 6. $NH_4^+ \rightarrow NH_3(aq) + H^+$ | 24.6, s$^{-1}$ | ref 29 |
| 7. $SO_2(g) \rightarrow SO_2$ (aq) | $\bar{c}\alpha/(4\Delta x)1.66 \times 10^{-21}$, s$^{-1}$ | this work |
| 8. $SO_2(aq) \rightarrow SO_2$ (g) | $\bar{c}\alpha/(4\Delta x H_{SO_2} RT)$, s$^{-1}$ | this work |
| 9. $SO_2(aq) + H_2O \rightarrow HSO_3^- + H^+$ | $3.4 \times 10^6$, s$^{-1}$ | ref 57 |
| 10. $HSO_3^- + H^+ \rightarrow SO_2(aq) + H_2O$ | $2.3 \times 10^8$, M$^{-1}$ s$^{-1}$ | ref 57 |
| 11. $SO_2(aq) + OH^- \rightarrow HSO_3^-$ | $1.1 \times 10^{10}$, M$^{-1}$ s$^{-1}$ | ref 27 |
| 12. $HSO_3^- \rightarrow SO_2(aq) + OH^-$ | $6.5 \times 10^{-3}$, s$^{-1}$ | ref 27 |
| 13. $H_2O \rightarrow H^+ + OH^-$ | $1.4 \times 10^{-3}$, s$^{-1}$ | ref 30 |
| 14. $H^+ + OH^- \rightarrow H_2O$ | $1.4 \times 10^{11}$, M$^{-1}$ s$^{-1}$ | ref 30 |

[a] Numerical values of the rate coefficients are for $T = 295$ K.

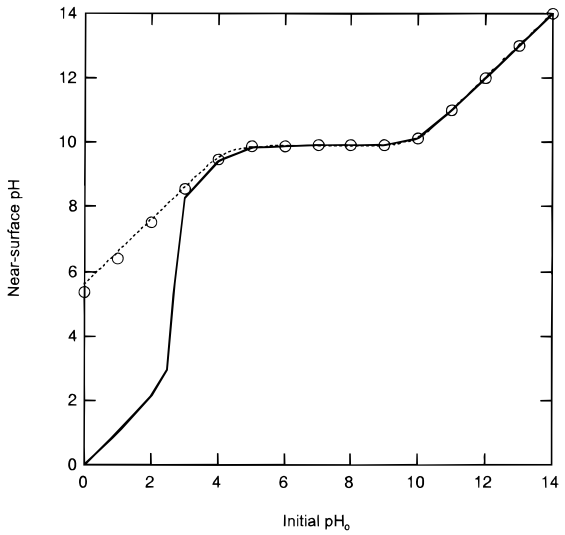


**Figure 12.** Near-surface pH as a function of initial $pH_0$. Solid line is a numerical calculation at gas−liquid contact time $t = 5$ ms. Dashed line is the equilibrium calculation based on eq A2-6. Circles are numerical calculations for a gas−liquid contact time of 300 s simulating equilibrium condition.

This model calculation provides a value for the total amount of $NH_3$ species that entered the liquid during time $t$. Therefore, the uptake coefficient $\gamma_0$ can be obtained by equating the total $NH_3$ species that entered per unit area to $(\bar{c}/4)n_g\gamma_0 t$. This way of computing $\gamma_0$ is in the good agreement (better than 4%) with the resistor model of Figures 1a and c.

**2. Codeposition of $NH_3$ with $SO_2$.** The uptake by droplets of $NH_3$ in the presence of gas-phase $SO_2$ is numerically calculated simply by taking into account additional reactions involving S(IV) species. The equilibrium conditions for $SO_2$ are

$$SO_2(g) \rightleftarrows SO_2(aq) \qquad \text{(A2-R1)}$$

$$SO_2(aq) + H_2O \rightleftarrows HSO_3^- + H^+ \qquad \text{(A2-R2)}$$

$$SO_2(aq) + OH^- \rightleftarrows HSO_3^- \qquad \text{(A2-R3)}$$

The solid line in Figure 11 was calculated via the above equations using the *Acuchem* program. The rate constants used in the calculations are listed in Table 4.

**Acknowledgment.** We thank Dr. Erick Swartz for his help in this work. Funding for this work was provided by the National Science Foundation Grant ATM-96-32599, the U.S. Environmental Protection Agency Grants R-821256-01-0 and R825253, and Department of Energy Grants DE-FG02-91ER61208, DE-FG02-94ER61854, and DE-FG02-98ER62581.

## References and Notes

(1) Jacob, D. J.; Hoffmann, M. R. *J. Geophys. Res.* **1983**, *88*, 6611.
(2) Finlayson-pitts, B. J.; Pitts, J. N. *Atmospheric Chemistry*; John Wiley and Sons: New York, 1986.
(3) Meng, Z.; Dabdub, D.; Seinfeld, J. H. *Science* **1997**, *277*, 116.
(4) Diau, E. W.-G.; Tso, D.-L.; Lee, Y.-P. *J. Phys. Chem.* **1990**, *94*, 5261.
(5) Warneck, P. *Chemistry of the Natural Atmosphere*; International Geophysics Series 41; Academic Press: San Diego, California, 1988.
(6) Ponche, J. L.; George, Ch.; Mirabel, Ph. *J. Atmos. Chem.* **1993**, *16*, 1.
(7) Bongartz, A.; Schweighoefer, S.; Roose, C.; Schurath, U. *J. Atmos. Chem.* **1995**, *20*, 35.
(8) Swartz, E.; Shi, Q.; Davidovits, P.; Jayne, J. T.; Worsnop, D. R.; Kolb, C. E. *J. Phys. Chem.* **1999**, *103*. 8824.
(9) Worsnop, D. R.; Zahniser, M. S.; Kolb, C. E.; Gardner, J. A.; Watson, L. R.; Van Doren, J. M.; Jayne, J. T.; Davidovits, P. *J. Phys. Chem.* **1989**, *93*, 1159.
(10) Jayne, J. T.; Worsnop, D. R.; Kolb, C. E.; Swartz, E.; Davidovits, P. *J. Phys. Chem.* **1996**, *100*, 8015.
(11) Robinson, G. N.; Worsnop, D. R.; Jayne, J. T.; Kolb, C. E.; Davidovits, P. *J. Geophys. Res.* **1997**, *103*, 3583.
(12) Shi, Q.; Li, Y. Q.; Davidovits, P.; Jayne, J. T.; Worsnop, D. R.; Mozurkewich, M.; Kolb, C. E. *J. Phys. Chem.* **1999**, *103*, 2417.
(13) Danckwerts, P. V. *Trans. Faraday Soc.* **1951**, *47*, 1014.
(14) Danckwerts, P. V. *Gas−Liquid Reactions*, McGraw-Hill: New York, 1970.
(15) Sherwood, T. K.; Pigford, R. L. *Absorption and Extraction*, 2nd ed.; McGraw-Hill: New York, 1952; p 329.
(16) Jayne, J. T.; Davidovits, P.; Worsnop, D. R.; Zahniser, M. S.; Kolb, C. E. *J. Phys. Chem.* **1990**, *94*, 6041.
(17) Hanson, D. R.; Ravishankara, A. R. *J. Phys. Chem.* **1994**, *98*, 5728.
(18) Hu, J. H.; Shi, Q.; Davidovits, P.; Worsnop, D. R.; Zahniser, M. S.; Kolb, C. E. *J. Phys. Chem.* **1995**, *99*, 8768.
(19) George, C.; Behnke, W.; Scheer, V.; Zetzsch, C.; Magi, L.; Ponche, J. L.; Mirabel, Ph. *Geophys. Res. Lett.* **1995**, *22*, 1505.
(20) Hanson, D. R. *J. Phys. Chem.* **1998**, *102*, 4794.
(21) Hanson, D. R. *J. Phys. Chem.* **1997**, *101*, 4998.
(22) Jayne, J. T.; Duan, S. X.; Davidovits, P.; Worsnop, D. R.; Zahniser, M. S.; Kolb, C. E. *J. Phys. Chem.* **1991**, *95*, 6329.
(23) Nathanson, G. M.; Davidovits, P.; Worsnop, D. R.; Kolb, C. E. *J. Phys. Chem.* **1996**, *100*, 13007.
(24) Mozurkewich, M.; McMurry, P. H.; Gupta, A.; Calvert, J. G. *J. Geophys. Res.* **1986**, *91*, 4163.
(25) Note that, in our earlier publications (refs 10, 16, and 35), $A^*_{eq}$ was the symbol used for the surface equilibrium constant.
(26) Note that the formulation of $\Gamma_c^{cx}$ assumes equilibrium between the liquid and surface species. If net uptake by other processes (i.e., $\Gamma_s^{rxn}$ or $\alpha$) is significant, then the steady-state concentration of $n_s^{cx}$ may be smaller than indicated in eq 15.
(27) Shi, Q. Ph.D. Thesis, Chemistry Department, Boston College, 1998.
(28) Houghton G. *J. Chem. Phys.* **1964**, *40(4)*, 1628.
(29) Emerson, M. T.; Ernest, G.; Kromhout, R. A. *J. Chem. Phys.* **1960**, *33(2)*, 547.
(30) Eigen, M. *Angew. Chem.* **1963**, *75*, 489; *Angew. Chem., Int. Ed. Engl.* **1964**, *3*, 1; *Pure Appl. Chem.* **1963**, *6*, 97.
(31) Fuchs, N. A.; Sutugin, A. G. *Highly Dispersed Aerosols*; Ann Arbor Science Publishers: Ann Arbor, 1970.
(32) Widmann, J. F.; Davis, E. J. *J. Aerosol Sci.* **1997**, *28*, 87.
(33) Hanson, D. R.; Ravishankara, A. R.; Lovejoy, E. R. *J. Geophys. Res.*, **1996**, *101*, 9063.
(34) Kee, R. J.; Miller, J. H.; Jefferson, T. H. *CHEMKIN: A Chemical Kinetics Code Package*; Sandia Laboratories: Albuquerque, NM, 1989.
(35) Jayne, J. T.; Duan, S. X.; Davidovits, P.; Worsnop, D. R.; Zahniser, M. S.; Kolb, C. E. *J. Phys. Chem.* **1992**, *96*, 5452.
(36) Duan, S. X.; Jayne, J. T.; Davidovits, P.; Worsnop, D. R.; Zahniser, M. S.; Kolb, C. E. *J. Phys. Chem.* **1993**, *97*, 2284.
(37) Castro, A.; Bhattacharyya, K.; Eisenthal, K. B. *J. Chem. Phys.* **1991**, *95(2)*, 1310.
(38) Karpovich, D. S.; Ray, D. *J. Phys. Chem. B* **1998**, *102*, 649.
(39) Sorina, G. A.; Minovich, V. M.; Efremova, G. D. *Zh. Obshch. Khim.* **1967**, *37*, 2150.
(40) Sherwood, T. K. *Ind. Eng. Chem.* **1925**, *17*, 745.
(41) Hales, J. M.; Drewes, D. R. *Atmos. Environ.* **1979**, *13*, 1133.
(42) Clegg, S. L.; Brimblecombe, P. *J. Phys. Chem.* **1989**, *93*, 7237.
(43) Davidovits, P.; Jayne, J. T.; Duan, S. X.; Worsnop, D. R.; Zahniser, M. S.; Kolb, C. E. *J. Phys. Chem.* **1991**, *95*, 6337.
(44) Lewis, G. N.; Randall, M.; Pitzer, K. S.; Brewer, L. *Thermodynamics*, 2nd ed.; McGraw-Hill: New York, 1961.
(45) Timmermans, J. *The Physicochemical Constants of Binary Systems in Concentrated Solutions*; Interscience: New York, 1960; Vol. 4, p 486.
(46) Donaldson, D. J. *J. Phys. Chem.* A **1999**, *103*, 62.
(47) Simonelli, D.; Baldelli, S.; Shultz, M. J. *Chem. Phys. Lett.* **1998**, *298*, 400.
(48) Chen, C.; Britt, H. I.; Boston, J. F.; Evans, L. B. *AIChE J.* **1979**, *24*, 820.
(49) Van Krevelen, D. W.; Hoftijzer, P. J.; Huntjens, F. J. *Rec. Trav. Chim. Pays-bas* **1949**, *68*, 191.
(50) Jayne, J. T.; Gardner, J. A.; Davidovits, P.; Worsnop, D. R.; Zahniser, M. S.; Kolb, C. E. *J. Geophys. Res.* **1990**, *95*, 20, 559.
(51) Crank, J. *Mathematics of Diffusion*, Oxford University Press: London, 1956.
(52) Braun, W.; Herron, T.; Kahaner, D. *Int. J. Chem. Kinet.* **1988**, *20*, 51.
(53) Maahs, H. G. *Heterogeneous Atmospheric Chemistry*; Schryer, D. R., Ed.; American Geophysical Union, Washington, DC, 1982; p 187.
(54) Bates, S. J.; Kirschman, H. D. *J. Am. Chem. Soc.* **1919**, *41*, 1991.
(55) Lide, D. R., Ed. *Handbook of Chemistry and Physics*, 73rd ed.; CRC Press: Boca Raton, FL, 1992; pp 6-10 and 8-42.
(56) Eigen, M.; Schoen, J. *Z Elektrochemie* **1955**, *59*, 483.
(57) Eigen, M.; Kustin, K.; Maass, G. *Z Phys. Chem. (Munich)* **1961**, *30*, 130.